

FILAMENT ORDERING AND CLUSTERING BY MOLECULAR MOTORS IN MOTILITY ASSAYS*

JAN KIERFELD

*Max Planck Institute of Colloids and Interfaces, Science Park Golm
14424 Potsdam, Germany*

PAVEL KRAIKIVSKI†

*Max Planck Institute of Colloids and Interfaces, Science Park Golm
14424 Potsdam, Germany*

REINHARD LIPOWSKY

*Max Planck Institute of Colloids and Interfaces, Science Park Golm
14424 Potsdam, Germany*

Received 30 July 2006

We study the cooperative behavior of cytoskeletal filaments in motility assays, in which immobilized motor proteins bind the filaments to a surface and actively pull them along this surface. Because of the repulsive interaction of filaments, the motor-driven dynamics of filaments leads to a nonequilibrium phase transition which generalizes the isotropic-nematic phase transition of the corresponding equilibrium system, the hard-rod fluid. Langevin dynamics simulations and analytical theory show that the motor activity enhances the tendency for nematic ordering. At high detachment forces of motors, we observe the formation of filament clusters because of blocking effects; at low detachment forces, cluster formation can be controlled by the density of inactive motors.

Keywords: Filaments; molecular motors; motility assays; pattern formation.

1. Introduction

The cytoskeleton of a living cell is a constantly re-organizing dynamic structure, which is necessary for cell division, cell motility, and force generation^{1,2}. Small forces generated by motor proteins provide one important mechanism that drives the dynamic processes in the cytoskeleton. As opposed to conventional polymer dynamics, which is governed by thermal fluctuations³, such motor forces give rise to an active filament dynamics, driven by a constant supply of mechanical energy by

*Paper presented at the conference on “Bio-Systems,” Berlin, June 26–29, 2006.

†Present address: University of Connecticut Health Center, 263 Farmington Avenue, Farmington, Connecticut 06030.

motor proteins, which hydrolyze adenine triphosphate (ATP). In order to understand the underlying principles of motor-driven filament dynamics it is necessary to study simple model systems *in vitro*. One such model system, which has been intensively studied *in vitro*, are bulk solutions of microtubules and two-headed kinesin motor proteins^{4,5,6}, in which the formation of patterns such as asters and vortices is observed. Theoretical studies of such patterns^{7,8,9,10,11} have used a coarse-grained continuum description with kinetic equations for filament density and orientation fields and a motor-density field. In these approaches it is inherently difficult to relate the macroscopic transport coefficients to the experimentally accessible microscopic parameters of the system. Based on experimental work on actin solutions containing myosin motor mini-filaments¹² it has also been suggested that the effect of motor activity can be described by an increased effective temperature in the nonequilibrium system.¹³

In this article, we consider the dynamics and pattern formation by many filaments in motility assays, in which the tails of motor proteins are adsorbed and anchored to a two-dimensional surface and filaments glide over this surface if the molecular motors are active. Motility or gliding assays are by now a standard tool to characterize motor proteins by analyzing the transport velocities of *single* filaments gliding over the substrate.¹⁴ We focus on the *cooperative* behavior of many filaments, which have a mutual repulsive interaction.¹⁵ Repulsive interactions originate from the steric interaction of filaments, which gives rise to an additional bending energy cost associated with each crossing of two filaments. This crossing energy cost can become large if the filaments are effectively confined to two dimensions by decreasing the height in the direction perpendicular to the surface below two filament diameters. In this case, a hard-core repulsion between filaments is effective. Because of their reduced dimensionality and the quenched motor concentration field, motility assays represent a slightly simpler model system in comparison to systems consisting of solutions of filaments and two-headed motor proteins. The equilibrium system corresponding to the confined motility assay with hard-core repulsion in the absence of motors is the two-dimensional hard-rod fluid, which exhibits an isotropic-nematic ordering transition above a critical density of filaments.^{16,17}

We show both numerically using a microscopic simulation model and by analytical arguments that the nematic ordering is enhanced by the presence of motor activity due to the combined effect of repulsive filament interactions and active forces exerted by the motors; see Fig. 1. Using previous results for the persistent motion of single filaments^{18,19,20} we extend the dynamic mean-field theory for nematic ordering²¹ to active systems. From the theoretical treatment, we derive the concept of an increased effective length, which successfully explains our simulation data for filaments with a hard-core repulsion characterized by an infinite filament crossing energy and allows to obtain the phase behavior in terms of the experimentally accessible microscopic model parameters. In the presence of a repulsive interaction characterized by a finite crossing energy for filaments, we discuss the

phase behavior using the additional concept of an effective temperature, which is also increased by the motor activity. Our results show that the concept of an effective temperature is rather subtle and does not apply in the limit of large energy barriers where the system becomes effectively athermal, i.e., is governed by steric interactions only.

In the presence of additional filament cross-linking molecules, we observe the formation of filament bundles similar to the bundling transition of filaments in thermal equilibrium.^{22,23} At high detachment forces of motors, we observe the formation of filament clusters because of blocking effects. Inactive motors increase the tendency to form clusters. At low detachment forces, cluster formation can therefore be controlled by the concentration of inactive motors.

2. Model

Our microscopic model for motility assays describes filament configurations, motor heads, and polymeric motor tails as separate degrees of freedom. One end of the motor tail is anchored to the substrate, and the motor head on the other end can bind to a filament in the correct orientation due to the tail flexibility. Once bound, the motor head moves along the filament thereby stretching the polymeric tail, which gives rise to a loading force acting both on the motor head and the attached filament. This force feeds back onto the motion of the bound motor head, which moves with a load-dependent motor velocity.^{24,25} Filaments follow an overdamped dynamics with external forces from the stretched motor tails and the repulsive filament-filament interaction, which are characterized by an energy barrier E_{ba} for filament crossing. In the limit of large crossing energies E_{ba} the filament interaction becomes a hard-core repulsion.

To proceed, let us consider N rigid filaments of length L (with index $i = 1, \dots, N$)

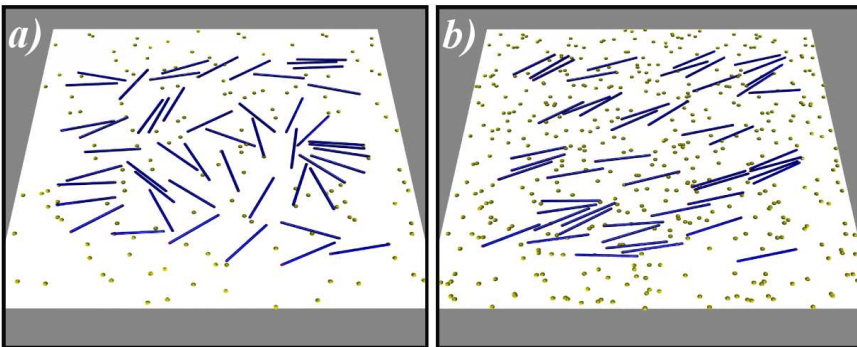


Fig. 1. Snapshots of rodlike filaments with hard-core repulsion on a motor coated substrate with randomly distributed motors and periodic boundary conditions. The filament concentration is $\rho = 2/L^2$, i.e., below the critical concentration of the equilibrium isotropic-nematic transition. For detachment forces $F_d = F_{st}$, we find (a) an isotropic phase at low motor surface density $\sigma \ell_m L = 0.03$ and (b) active nematic ordering at high motor surface density $\sigma \ell_m L = 0.09$.

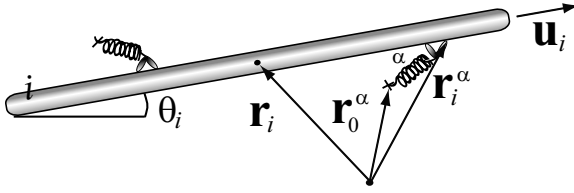


Fig. 2. Schematic top view of a filament i in the motility assay with two motors attached. \mathbf{r}_i is the filament's center of mass, θ_i and \mathbf{u}_i its orientational angle and unit vector, respectively. The attached motor α is anchored at \mathbf{r}_0^α , and its head is positioned at \mathbf{r}_i^α .

on a planar two-dimensional surface. The configuration of filament i can then be specified by the two-dimensional vector \mathbf{r}_i for its center of mass and by the angle θ_i or the unit vector $\mathbf{u}_i = (\cos \theta_i, \sin \theta_i)$ for its orientation; see Fig. 2. The filament is subject to forces \mathbf{F}_i^α from N_i attached motors (with index $\alpha = 1, \dots, N_i$) with motor heads positioned at \mathbf{r}_i^α . Each such force arises from the polymeric tail of motor α , which is stretched by the directed motion of the motor head on the filament, as described below. The motor tail is anchored at \mathbf{r}_0^α and the head position is \mathbf{r}_i^α . We model the polymeric tail as a freely jointed chain such that \mathbf{F}_i^α is obtained by inverting the force-extension relation of a freely jointed chain.^a In addition to motor forces, the filaments are subject to interaction forces \mathbf{F}_{ij} arising from the purely repulsive interactions between filaments i and j ²⁷. If two filaments of diameter D cross each other, these forces give rise to a crossing energy cost E_{ba} .

Under the influence of the motor forces \mathbf{F}_i^α and the interaction forces \mathbf{F}_{ij} each filament i performs an overdamped translational motion, which is described by the stochastic Langevin-type equation of motion

$$\Gamma \cdot \partial_t \mathbf{r}_i = \sum_{\alpha=1}^{N_i} \mathbf{F}_i^\alpha + \sum_{j=1}^N \mathbf{F}_{ij} + \zeta_i, \quad (1)$$

where

$$\Gamma \equiv \Gamma_{\parallel} \mathbf{u}_i \otimes \mathbf{u}_i + \Gamma_{\perp} (\mathbf{I} - \mathbf{u}_i \otimes \mathbf{u}_i), \quad (2)$$

is the matrix of translational friction coefficients, which is given by friction coefficients Γ_{\parallel} and Γ_{\perp} for motion parallel and perpendicular to the filament orientation \mathbf{u}_i , respectively, and $\zeta_i(t)$ are the Gaussian distributed thermal random forces.³ In eq. (2), \mathbf{I} is the unit matrix and \otimes the dyadic vector product. The thermal noise $\zeta_i(t)$ has correlations $\langle \zeta_i(t) \otimes \zeta_j(t') \rangle = 2T\Gamma \delta_{ij} \delta(t - t')$.

In addition to filament translation, motor and interaction forces give also rise to the torques $M_i^\alpha \equiv |(\mathbf{r}_i^\alpha - \mathbf{r}_i) \times \mathbf{F}_i^\alpha|$ and M_{ij} , respectively²⁷. These torques lead to

^aIf the motor tail is anchored at \mathbf{r}_0^α , the force $-\mathbf{F}_i^\alpha$ is pointing in the direction $\Delta \mathbf{r}^\alpha \equiv \mathbf{r}_i^\alpha - \mathbf{r}_0^\alpha$ and $|\Delta \mathbf{r}^\alpha|/L_m = f_{\text{FJC}}(|\mathbf{F}_i^\alpha|b_m/T)$, where L_m is the contour and b_m the monomer length of the polymeric motor tail, and $f_{\text{FJC}}(x) \equiv 1/\tanh x - 1/x$, cf. Ref. 26.

an overdamped rotational dynamics, which is described by

$$\Gamma_\theta \partial_t \theta_i = \sum_{\alpha=1}^{N_i} M_i^\alpha + \sum_{j=1}^N M_{ij} + \zeta_{\theta,i}, \quad (3)$$

where Γ_θ is the rotational friction coefficient and $\zeta_{\theta,i}(t)$ is a Gaussian distributed thermal random torque. The thermal torque $\zeta_{\theta,i}(t)$ has correlations $\langle \zeta_{\theta,i}(t) \zeta_{\theta,j}(t') \rangle = 2T\Gamma_\theta \delta_{ij} \delta(t-t')$.

Note that all friction coefficients Γ_\parallel , Γ_\perp and Γ_θ are identical to those of the passive filament dynamics, see Ref. 3.

The dynamics of motor heads is described by a deterministic equation of motion

$$\partial_t x_i^\alpha = v(\mathbf{F}_i^\alpha), \quad (4)$$

where $|x_i^\alpha| \leq L/2$ defines the position of the motor α along the rod i , i.e., $\mathbf{r}_i^\alpha = \mathbf{r}_i + x_i^\alpha \mathbf{u}_i$, and the filament polarity is such that the motor head moves in the direction \mathbf{u}_i . The motor velocity v is a function of the loading force \mathbf{F}_i^α which builds up due to stretching of the motor tail. We use a force-velocity relation with a maximum value v_{\max} for forces $\mathbf{F}_i^\alpha \cdot \mathbf{u}_i \geq 0$ pulling the motor forward, a linear decrease for forces $\mathbf{F}_i^\alpha \cdot \mathbf{u}_i < 0$ pulling the motor backwards, and $v = 0$ for $\mathbf{F}_i^\alpha \cdot \mathbf{u}_i < -F_{st}$, where F_{st} is the stall force.^{24,25}

We assume that the motor binds to the filament when the distance between the anchored end of the motor tail at \mathbf{r}_0^α and the filament is smaller than a capture radius ℓ_m . Apart from the stall force F_{st} the motor is also characterized by its detachment force F_d , above which the unbinding rate of the motor head becomes large. For simplicity we assume in our model that the motor head detaches whenever the force F_i^α exceeds a threshold value F_d . We consider the case of processive motors with a high duty ratio close to unity, i.e., motors detach from a filament only if they reach the filament end or if the total force becomes larger than the detachment force F_d .

3. Simulation

Using the above model we performed simulations of gliding assays for a random distribution of motors with a surface density σ and periodic boundary conditions. At each time step Δt , we update the motor head positions x_i^α and filament positions and orientations using the discretized versions of the equations of motions described above. The parameter values that we choose for the simulations are comparable with experimental data on assays for conventional kinesin. The simulation results presented in Figs. 1 and 3 have been obtained for quadratic assays of area $25\mu\text{m}^2$ with filaments of length $L = 1\mu\text{m}$ and diameter $D = L/40$ at room temperature $T \simeq 4 \times 10^{-3} \text{pN} \mu\text{m}$. The friction coefficients are taken to be $\Gamma_\perp = 2\Gamma_\parallel = 4\pi\eta L / \ln(L/D)$ and $\Gamma_\theta = \Gamma_\parallel L^2/6$, where η is the viscosity of the surrounding liquid.³ We use a value $\eta = 0.5\text{pN s}/\mu\text{m}^2$ much higher than the viscosity of water, $\eta_{\text{water}} \sim 10^{-3} \text{pN s}/\mu\text{m}^2$, which allows to take larger simulation time steps. We checked that this does not affect results. We use a maximum motor speed of $v_{\max} = 1\mu\text{m/s}$ and a stall force of

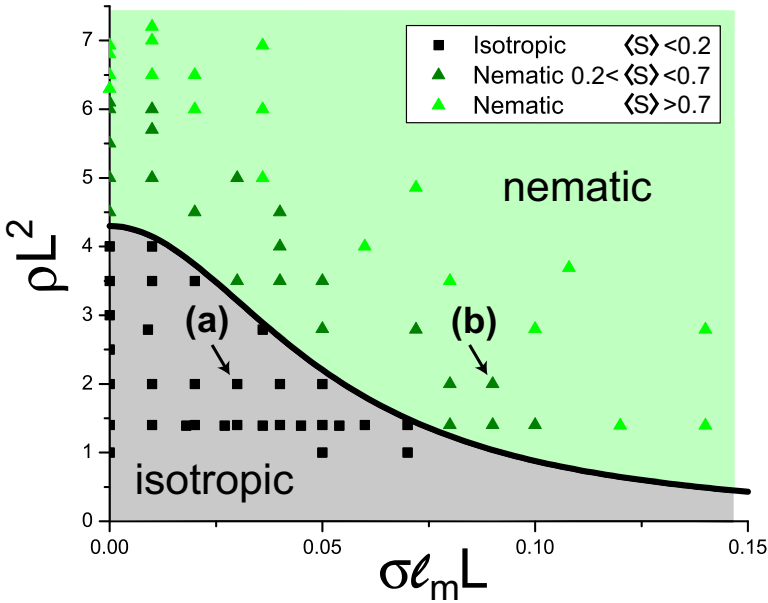


Fig. 3. The phase diagram for the gliding assay as a function of the dimensionless filament density ρL^2 and the dimensionless surface motor density $\sigma \ell_m L$ for detachment force $F_d = F_{st}$, and $L/\ell_m = 100$, and a hard-core repulsion between filaments. All data points correspond to separate simulation runs, the two arrows (a) and (b) to the snapshots in Fig. 1. If the average order parameter $\langle S \rangle < 0.2$, the system is in the isotropic phase (black squares, grey area), if $\langle S \rangle > 0.2$ it is in the nematic phase (green triangles, green area). The solid line represents the analytical result as given by (7).

$F_{st} = 5\text{pN}$. The capture radius for motor proteins is $\ell_m = 10^{-2}\mu\text{m}$ and the length of the fully stretched motor tail $L_m = 5 \times 10^{-2}\mu\text{m}$. Each data point in the phase diagram in Figs. 3 and 4 corresponds to a simulation run over 10^6 time steps. In the simulation we take time steps $\Delta t = 10^{-3}\text{s}$ such that 10^6 simulation time steps correspond to 10^3s .

4. Phase behavior for hard-core filament repulsion

First we consider the phase behavior in the limit of a large filament crossing energy E_{ba} , where a hard-core repulsion between filaments is effective. Motor activity then strongly modifies the nematic ordering of rigid filaments of length L in a motility assay. Therefore, both the rod density ρ and the motor density σ are essential in order to determine the phase behavior, which can be described in the plane of the two dimensionless parameters ρL^2 and $\sigma \ell_m L$ as shown in Fig. 3. Nematic ordering in a system of N filaments can be characterized by the time averages of the order parameter $S \equiv \sum_{i \neq j} \cos(2(\theta_i - \theta_j))/N(N-1)$. In an infinite system, we expect $\langle S \rangle = 0$ in the isotropic phase and $\langle S \rangle = 1$ for perfect nematic order. In equilibrium, i.e., in the absence of motors ($\sigma = 0$) we find a continuous isotropic-nematic

transition at a critical density $\rho_{c,0} \simeq 4.3/L^2$ in the simulation, which is in good agreement with the analytic result $\rho_c = 3\pi/2L^2$ based on Onsager's theory for the two-dimensional hard-rod fluid.¹⁷ The equilibrium transition is found numerically from the inversion point of the curve $\langle S \rangle = \langle S \rangle(\rho)$ for a value $\langle S \rangle \simeq 0.2$, which we also use as the threshold value for active nematic ordering if motors are present ($\sigma > 0$), see Fig. 4. Snapshots of the actively driven system in the isotropic and nematic phase are shown in Figs. 1(a) and (b), respectively. In the resulting phase diagram Fig. 3, the critical density ρ_c for active nematic ordering *decreases* with increasing motor density, i.e., nematic ordering is favored if more energy is fed into the system. The transition is continuous also for non-zero motor-density, see the order parameter plots in Fig. 4.

Each driven filament gives a contribution $\mathbf{J}_i = N^{-1}\rho v_F \mathbf{u}_i$ to the filament current, where v_F is the mean filament velocity. This velocity can be obtained by simultaneously equating (i) the filament friction force with the total motor driving force and (ii) the filament velocity with the motor velocity in the steady state, which gives $v_F = v_{\max}(1 + \Gamma_{\parallel} v_{\max} \langle d_m \rangle / LF_{st})^{-1}$. In the presence of motor activity and in the nematic phase, the contributions to the total filament current become correlated along a preferred direction given by the unit vector \mathbf{n} leading to a non-vanishing expectation value $\sum_{i \neq j} \langle (\mathbf{J}_i \cdot \mathbf{J}_j)^2 \rangle / N(N-1) = N^{-4} \rho^4 v_F^4 \langle S \rangle$. This gives rise to two macroscopic filament currents $\langle \mathbf{J}_{\pm \mathbf{n}} \rangle = \pm \rho v_F \mathbf{n} / 2$ of opposite directions $\pm \mathbf{n}$ with zero total current, $0 = \sum_i \langle \mathbf{J}_i \rangle = \langle \mathbf{J}_{\mathbf{n}} \rangle + \langle \mathbf{J}_{-\mathbf{n}} \rangle$. The existence of such macroscopic currents is characteristic for a non-equilibrium phase. These currents vanish (i) for small motor density, i.e., upon approaching the vertical axis $\sigma \ell_m L = 0$ in the phase diagram Fig. 3 and (ii) upon approaching the isotropic-nematic phase boundary in the phase diagram Fig. 3, which is given by (7).

The motion of a filament is characterized by stochastic switching between rotational and translational diffusion if no motors are attached, directed translation in rotationally diffusing directions if one motor is attached, and directed translation if two or more motors are attached. The relative frequency of these types of motion depends on the mean distance $\langle d_m \rangle$ between bound motors and, thus, on the surface motor concentration σ .¹⁸ For high motor concentrations a filament has two or more bound motors on average and $\langle d_m \rangle \sim 1/\sigma \ell_m$. The single filament performs a persistent walk with a persistence length¹⁸

$$\xi_p = \frac{L + 2\langle d_m \rangle}{L + 3\langle d_m \rangle} \frac{L^3}{9\ell_m^2} \left(e^{L/\langle d_m \rangle} - 1 - \frac{L}{\langle d_m \rangle} \right) \quad (5)$$

corresponding to a persistence time $t_p = \xi_p/v_F$. A coarse-graining in time by averaging over time intervals of one persistence time t_p leads to an effective random walk of a single filament. On time scales larger than t_p the dynamics of a filament is again described by a diffusion equation as for passive dynamics. After coarse-graining to one persistence time we can adapt the mean-field treatment of the hard-rod fluid²¹ to obtain an analytical result for the phase boundary.¹⁵ The effective excluded area governing the steric interaction between two motor-driven filaments with center of

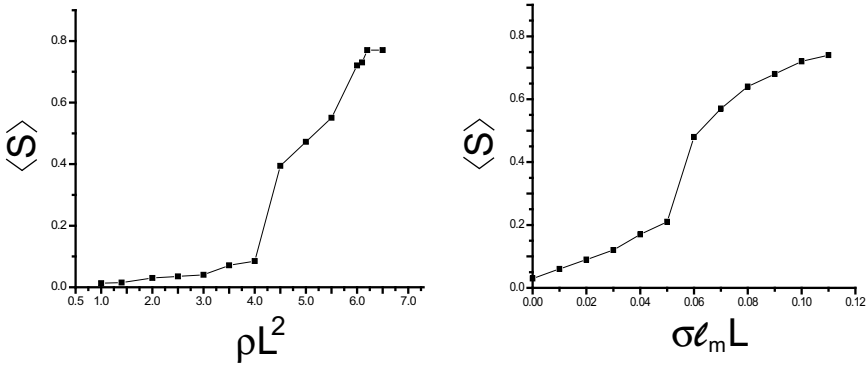


Fig. 4. Plots of the order parameter $\langle S \rangle$ crossing the isotropic-nematic transition. (Left) The order parameter as a function of the dimensionless filament density ρL^2 at zero motor density. The transition point is at $\rho L^2 = 4.3$. (Right) The order parameter as a function of the dimensionless motor density $\sigma \ell_m L$ for a filament density $\rho L^2 = 2$ and $L/\ell_m = 100$ (which is the same as for the snapshots in Fig. 1 of the article). The transition point is at $\sigma \ell_m L = 0.047$. In each plot we can identify the transition points as inflection points of the order parameter curve. Each data point in the order parameter plots corresponds to the average value of the order parameter taken over 10^6 time steps.

masses and orientations (\mathbf{r}, \mathbf{u}) and $(\mathbf{r}', \mathbf{u}')$ on the surface of the motility assay is

$$A_{\text{exc}} = |\mathbf{u} \times \mathbf{u}'| \iint_{-L/2}^{L/2+\xi_p} d\xi d\eta \Theta_L(\xi - \eta) \delta(\mathbf{r} - \mathbf{r}' + \mathbf{u}\xi + \mathbf{u}'\eta) = |\mathbf{u} \times \mathbf{u}'| L(L + \xi_p), \quad (6)$$

where $\Theta_L(\xi - \eta)$ equals one if $|\xi - \eta| < L/2$ and zero otherwise. Performing an analogous stability analysis as in Ref. 21 using this effective excluded area we finally obtain the critical filament density of the active isotropic-nematic transition,

$$\rho_c = c/L[L + \xi_p(\langle d_m \rangle, \ell_m, L)] \quad (7)$$

with $c = 3\pi/2$ from the analytical mean-field calculation.^b

In the absence of motors we have $\xi_p = 0$ and the result (7) reduces to the equilibrium result of Ref. 17. Using the result (5) for the persistence length $\xi_p = \xi_p(\langle d_m \rangle, \ell_m, L)$, we obtain an explicit expression of the isotropic-nematic phase boundary in the active system in terms of the microscopic parameters, which is in good agreement with all simulation data, see Fig. 3. Beyond mean-field, we expect a larger numerical prefactor c in (7) but the same parameter dependence.

The result (7) corresponds to an *effectively increased filament length* $L_{\text{eff}} = \sqrt{L(L + \xi_p)}$ as compared to the equilibrium system, which explains that motor activity actually favors nematic ordering. In deriving the phase boundary (7), we have established a mapping of the nonequilibrium driven system onto an equilibrium

^bThe analogous calculation for filaments moving in a quenched array of motors in three spatial dimensions gives a critical filament density $\rho_c^{3d} = c^{3d}/DL[L + \xi_p^{3d}]$ for active nematic ordering, where $\xi_p^{3d} = \xi_p \pi^2 L^2 / 4\ell_m^2$ and $c^{3d} = 4\pi/3$.

system with larger effective filament length. This mapping only applies within the isotropic phase as it is based on the statistical properties of the motion of a *single* filament (or *non-interacting* filaments) but can be used to calculate the stability boundary (7) of the isotropic phase.

5. Phase behavior for finite filament crossing energy

The motor-activity also increases the effective diffusion constant of single filaments to $D_{\text{eff}} \sim D_F + \xi_p v_F$ ^{18,19,20} from its bare value D_F . Thus, using the Einstein relation³ $D_{\text{eff}} = T_{\text{eff}}(\Gamma_{\parallel}^{-1} + 2\Gamma_{\perp}^{-1})/3$ we might define an increased effective temperature $T_{\text{eff}} \sim T + 3\xi_p v_F / (\Gamma_{\parallel}^{-1} + 2\Gamma_{\perp}^{-1})$ for the isotropic phase. For steric filament interactions, i.e., in the limit of an athermal system with infinite crossing energy E_{ba} , this effective temperature does *not* influence the excluded area (6) and, thus, the phase behavior. For a finite filament crossing energy E_{ba} , however, the suppression of filament crossings depends on the ratio E_{ba}/T_{eff} . Filament crossing remains rare in the limit of large $E_{ba}/T_{\text{eff}} \gg 1$, becomes increasingly frequent upon reducing E_{ba}/T_{eff} and, finally, filaments become effectively non-interacting for $E_{ba}/T_{\text{eff}} \ll 1$. This effect can be analytically described by deriving the appropriate excluded volume for a finite filament crossing energy, which gives $A_{\text{exc}} = |\mathbf{u} \times \mathbf{u}'| L(L + \xi_p)(1 - e^{-E_{ba}/T_{\text{eff}}})$, and we expect a modified phase boundary for the active nematic ordering at a critical density $\rho_c = c[L(L + \xi_p)(1 - e^{-E_{ba}/T_{\text{eff}}})]^{-1}$. At high motor density, where ξ_p becomes large, the phase boundary approaches a finite value $\rho_{c,\infty} \approx 3cv_F / (\Gamma_{\parallel}^{-1} + 2\Gamma_{\perp}^{-1})E_{ba}$.

6. Bundle formation

In thermal equilibrium, i.e., in the absence of motor forces, filaments can undergo a discontinuous bundling transition in the presence of additional short-range attractive interactions mediated by crosslinkers.^{22,23} We observe a similar transition for filaments in the motility assay if we add crosslinking molecules with two adhesive end groups to our microscopic simulation model.

In order to include such linker molecules into the simulation, we discretize each filament into segments of length a_{\parallel} . At each segment a crosslinking molecule can adsorb with one sticky end. We choose the discretization length equal to the filament diameter, $a_{\parallel} = D$, and consider a hard-core interaction between linkers, i.e., each adsorption site can be occupied by at most one linker molecule. Upon adsorption of one linker end on a filament the crosslinker gains an adhesive energy $a_{\parallel}W < 0$. If an empty adsorption site on a second filament approaches the adsorbed linker end, the other end domain of the crosslinker can gain an energy $a_{\parallel}W + W_{\text{FJC}}(|\Delta \mathbf{r}_{ij,k}|)$ upon adsorbing to this empty site: The first contribution is again the adhesive energy of a linker end group, whereas the second contribution is the stretching energy of the polymeric linker domain of the crosslinking molecule, which is modeled as a freely jointed chain. Integrating the force-extension relation of a freely jointed chain,²⁶

we find $W_{\text{FJC}}(|\Delta\mathbf{r}_{ij,k}|) \simeq (TL_l/b_l)w_{\text{FJC}}(|\Delta\mathbf{r}_{ij,k}|/L_l)$, where L_l is the contour, b_l is the monomer length of the polymeric linker domain, and $w_{\text{FJC}}(x) \equiv -\ln(1-x) - x + x^2$. After connecting two filaments, this polymeric spring connection exerts additional forces onto each of the two filaments. The adsorption and desorption of linker-domains is simulated using a Monte-Carlo-like algorithm.

Using this simulation model for additional crosslinking molecules we observe the formation of filament bundles above a critical crosslinker concentration, similar to the corresponding equilibrium system.^{22,23} Simulations also indicate that these filament bundles dissolve if the motor density and, thus, the effective temperature is sufficiently increased.

7. Cluster formation

Mutual blocking of filaments can lead to kinetically arrested filament clusters as shown in Fig. 5. We find that stable clusters appear if the detachment force F_d is large compared to the stall force F_{st} such that the maximal force transmitted to a filament through collisions does not lead to detachment of the filament and dissolution of the cluster. Because collisions between filaments are exceptional in the isotropic phase, clusters occur primarily in the nematic phase region.

The formation of such clusters is sensitively controlled by the presence of inactive motors, whose motor heads attach to filaments but which are inactive, either because of a lack of ATP or because they are dysfunctional. Such inactive motors simply bind filaments to the anchoring point of the motor tail without pulling them forward. Our simulations indicate that inactive motors increase the tendency of the system to form clusters. At low detachment forces, cluster formation can therefore be controlled by the concentration of inactive motors. In a crude estimate we can consider the maximal pushing force that a filament in a cluster can generate as $F_{st}L/\langle d_{m,ac} \rangle$, where $\langle d_{m,ac} \rangle \sim 1/\sigma_{ac}\ell_m$ is the mean distance between bound ac-

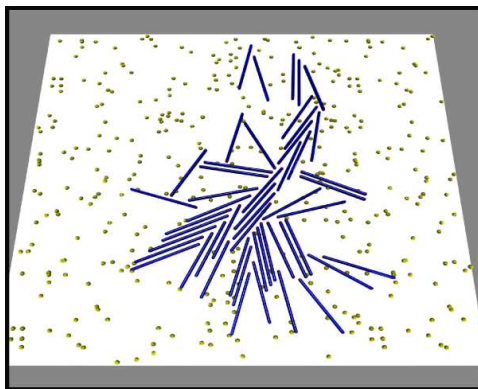


Fig. 5. Snapshot of a cluster of mutually blocking filaments for large detachment force $F_d = 10F_{st}$ using otherwise the same parameters as in Fig. 1(b) [$\rho = 2/L^2$, $\sigma\ell_m L = 0.09$].

tive motors on a filament and σ_{ac} the surface concentration of active motors. This pushing force is only generated by active motors. On the other hand, the maximal force for detachment of a filament in a cluster is $F_d L(1/\langle d_{m,ac} \rangle + 1/\langle d_{m,in} \rangle)$, where $\langle d_{m,in} \rangle \sim 1/\sigma_{in} \ell_m$ is the mean distance between bound inactive motors on a filament and σ_{in} the surface concentration of inactive motors. Detachment has to happen against active *and* inactive motors binding a filament to the surface. Equating these forces we find a criterion $F_{st}/F_d < 1 + \langle d_{m,ac} \rangle / \langle d_{m,in} \rangle = 1 + \sigma_{in} / \sigma_{ac}$ for cluster formation, which demonstrates that a high ratio of inactive motors on the surface, $\sigma_{in} / \sigma_{ac} \gg 1$, can promote the formation of clusters even for stall forces larger than detachments forces, i.e., even if $F_{st}/F_d > 1$.

8. Experimental realization

Confinement of filaments to strictly two dimensions is hard to realize experimentally but it has been observed that microtubules in a dynein motility assay exhibit hard-core interactions also in the absence of such a confinement.²⁸ Our results for finite filament crossing energies indicate that a small mean filament velocity v_F favors the nematic phase if filament crossing is possible.

Alternatively, we propose to consider a three-dimensional filament solution that is confined between two plates with anchored motors. The motor activity can induce an active *surface* nematic ordering of the filaments, which eventually propagates into the bulk if the filament density is sufficiently close to the critical density of the equilibrium Onsager transition in three dimensions.

9. Conclusion

We have presented simulations and a theoretical description of the phase behavior of filaments in a two-dimensional motility assay. The corresponding equilibrium system is the two-dimensional hard-rod fluid, which exhibits an isotropic-nematic phase transition. We have found that actively driven systems undergo an analogous phase transition and the motor activity *enhances* the tendency for nematic ordering. A similar enhancement is found in three-dimensional active filament solutions.⁸ For the two-dimensional motility assays we have quantitatively determined the phase boundary (7) for active nematic ordering by motors in terms of experimentally accessible microscopic model parameters. For high motor detachment forces $F_d \gg F_{st}$, we also find kinetically arrested filament clusters within the nematic phase region.

Acknowledgments

This work was supported by the EC Sixth Framework Programme (as part of the STREP Active Biomics contract No. NMP4-CT-2004-516989).

References

1. D. Bray, *Cell movements : from molecules to motility* (Garland Publishers, New York, 2001).
2. J. Howard, *Mechanics of Motor Proteins and the Cytoskeleton* (Sinauer Associates, Inc., Sunderland, 2001).
3. M. Doi and S.F. Edwards, *The Theory of Polymer Dynamics* (Clarendon, Oxford, 1986).
4. F.J. Nédélec, T. Surrey, A.C. Maggs, and S. Leibler, *Nature* **389**, 305 (1997).
5. T. Surrey, M.B. Elowitz, P.-E. Wolf, F. Yang, F. Nédélec, K. Shokat, and S. Leibler, *Proc. Natl. Acad. Sci. USA* **95**, 4293 (1998).
6. T. Surrey, F. Nédélec, S. Leibler, and E. Karsenti, *Science* **292**, 1167 (2001).
7. H.Y. Lee and M. Kardar, *Phys. Rev. E* **64**, 056113 (2001).
8. T.B. Liverpool and M.C. Marchetti, *Phys. Rev. Lett.* **90**, 138102 (2003).
9. K. Kruse, J.F. Joanny, F. Jülicher, J. Prost, and K. Sekimoto, *Phys. Rev. Lett.* **92**, 078101 (2004).
10. I.S. Aranson and L.S. Tsimring, *Phys. Rev. E* **71**, 050901(R) (2005).
11. F. Ziebert and W. Zimmermann, *Phys. Rev. E* **70**, 022902 (2004).
12. D. Humphrey, C. Duggan, D. Saha, D. Smith, and J. Käs, *Nature* **416**, 413 (2002).
13. T.B. Liverpool, A.C. Maggs, and A. Ajdari, *Phys. Rev. Lett.* **86**, 4171 (2001).
14. J. Scholey, *Motility assays for motor proteins*, *Meth. Cell Biology* **39**, (Academic Press, New York, 1993).
15. P. Kraikivski, R. Lipowsky, and J. Kierfeld, *Phys. Rev. Lett.* **96**, 258103 (2006).
16. L. Onsager, *Ann. N.Y. Acad. Sci.* **51**, 627 (1949).
17. R.F. Kayser and H.J. Raveché, *Phys. Rev. A* **17**, 2067 (1978).
18. T. Duke, T.E. Holy, and S. Leibler, *Phys. Rev. Lett.* **74**, 330 (1995).
19. M.R. Faretta and B. Basetti, *Europhys. Lett.* **41**, 689 (1998).
20. F. Gibbons, J.-F. Chauwin, M. Despósito, and J.V. José, *Biophys. J.* **80**, 2515 (2001).
21. M. Doi, T. Shimada, and K. Okano, *J. Chem. Phys.* **88**, 4070 (1988); T. Shimada, M. Doi, and K. Okano, *J. Chem. Phys.* **88**, 7181 (1988).
22. J. Kierfeld, T. Kühne and R. Lipowsky, *Phys. Rev. Lett.* **95**, 038102 (2005).
23. J. Kierfeld and R. Lipowsky, *Europhys. Lett.* **62**, 285 (2003); J. Kierfeld and R. Lipowsky, *J. Phys. A: Math. Gen.* **38**, L155 (2005).
24. C.M. Coppin, D.W. Pierce, L. Hsu, R.D. Vale, *Proc. Natl. Acad. Sci. USA* **94**, 8539 (1997).
25. S.M. Block, C.L. Asbury, J.W. Shaevitz, M.J. Lang, *Proc. Natl. Acad. Sci. USA* **100**, 2351 (2003).
26. J. Kierfeld, O. Niamploy, V. Sa-yakanit, and R. Lipowsky, *Eur. Phys. J. E* **14**, 17 (2004).
27. See auxiliary EPAPS Document No. E-PRLTAO-97-024627 of Ref. 15.
28. Kazuhiro Oiwa, *private communication*.